JGR Planets

RESEARCH ARTICLE
10.1029/2019JE006217

Key Points:
- We have measured the hardness of CO_2 ice in Martian temperatures
- We derived the corresponding yield strength values
- Under Martian conditions CO_2 ice is slightly weaker than H_2O ice

Correspondence to:
A. Hagermann,
axel.hagermann@stir.ac.uk

Citation:
Kaufmann, E., Attree, N., Bradwell, T., & Hagermann, A. (2020). Hardness and yield strength of CO_2 ice under Martian temperature conditions. *Journal of Geophysical Research: Planets*, *125*, e2019JE006217. https://doi.org/10.1029/2019JE006217

Received 26 SEP 2019
Accepted 3 MAR 2020

Author Contributions
Funding Acquisition: T. Bradwell, A. Hagermann
Methodology: E. Kaufmann
Software: N. Attree
Writing - Original Draft: E. Kaufmann, N. Attree, A. Hagermann
Formal Analysis: N. Attree
Investigation: E. Kaufmann, N. Attree
Resources: T. Bradwell, A. Hagermann
Writing - review & editing: T. Bradwell

Hardness and Yield Strength of CO_2 Ice Under Martian Temperature Conditions

E. Kaufmann[1], **N. Attree**[1], **T. Bradwell**[1], **and A. Hagermann**[1]

[1]Faculty of Natural Sciences, University of Stirling, Stirling, UK

Abstract Although ice fracturing and deformation is key to understanding some of the landforms encountered in the high-latitude regions on Mars and on other icy bodies in the solar system, little is known about the mechanical characteristics of CO_2 ice. We have measured the hardness of solid CO_2 ice directly in the laboratory with a Leeb hardness tester and calculated the corresponding yield strength. We have also measured the hardness of water ice by the same method, confirming previous work. Our results indicate that CO_2 ice is slightly weaker, ranging between Leeb ~200 and 400 (~10 and 30 MPa yield strength, assuming only plastic deformation and no strain hardening during the experiment), for typical Martian temperatures. Our results can be used for models of CO_2 ice rupture (depending on the deformation timescales) explaining surface processes on Mars and solar system icy bodies.

Plain Language Summary We have measured the hardness and calculated the strength of dry (carbon dioxide) ice. It is slightly weaker than water ice in the temperature range that can be found on Mars. Our results can be used in models of how surface features on Mars and on other icy surfaces in the solar system are formed.

1. Introduction

The surfaces of numerous solar system bodies are wholly or partly covered with water and/or carbon dioxide ice whose dynamics play a key role in the shaping of planetary landforms. Responding to gravitational, tidal, and other forces, ice may flow, or fracture, affecting the morphology of surfaces composed of both volatile and nonvolatile material. While the mechanical properties of water ice, whose dynamical behavior affects large portions of the Earth, are reasonably well understood, very little attention has been paid to the mechanical properties of CO_2 ice, which plays an important role on bodies throughout the solar system. On Mars, CO_2 covers the southern pole and CO_2 ice seems to be responsible for numerous enigmatic landforms that can be found in regions such as the so-called cryptic terrain (Kieffer et al., 2000) or the Swiss-cheese terrain (e.g., Malin et al., 2001). Specifically, quantifying the dynamic behavior of CO_2 ice is important to address questions relating to the processes resulting in araneiforms. These are channel-like features scoured in the polar regolith by hypothesized gas flow under a layer of CO_2 ice (Kieffer, 2007). When this gas pressure exceeds the—unknown—rupture strength of the overlying ice, gas and regolith can be ejected onto the surface, creating plumes and playing an important role in dust transportation on Mars. CO_2 ice strength is therefore a key parameter in understanding these processes, but, to date, whenever hardness/strength data were needed to explain CO_2 ice-related phenomena on Mars, authors have had to find work-arounds. Modeling gas activity of CO_2-covered surfaces on Mars, Portyankina et al. (2010) pointed out that considerable uncertainties are related to the poorly constrained mechanical characteristics of CO_2 ice and so they base their model on water ice parameters. Portyankina et al. (2012) took the same approach and point out that the fracturing part of their model "is highly uncertain mostly because of the lack of measurements of the mechanical properties of CO_2 ice." Some experimental evidence does exist: Nye et al. (2000) were able to conclude, based on Durham et al's (1999) deformation experiments of CO_2 ice, that Mars's south polar cap is unlikely to consist of pure CO_2 ice because it would not be mechanically stable. Clark and Mullin (1976) measured the flow law for solid CO_2 ice and found it to be one tenth to one third as strong as water ice under equivalent Martian conditions. However, similar to Durham et al's (1999) experiments, this represents the material behavior under low strain rate viscous flow, rather than the tensile, yield, or compressive strength values more relevant for sudden events such as fracturing. Beyond Mars, understanding the strength of CO_2 ice is relevant to the mechanical properties of icy regoliths on the surfaces and interiors of outer solar system objects such as comets and Kuiper belt objects.

We have measured the hardness of compact CO_2 ice as a function of temperature, using a commercial Leeb hardness tester. We discuss the results of this test (a local impact hardness in the high strain rate regime) in the context of material deformation models at different scales and Martian temperature conditions and the similar existing measurements made for water ice by Henderson et al. (2019). Our results can be used to inform models of CO_2 ice-related landscape evolution on Mars and provide important parameters for understanding the mechanical behavior of CO_2-covered surfaces elsewhere in the solar system.

2. Method

The Leeb rebound hardness test method is a dynamic test procedure that was developed as a flexible alternative to traditional hardness testing methods such as the Vickers method (Smith & Sandland, 1925). These methods usually require fixed workstations and can cause damage to the test object. The use of a portable Leeb hardness tester usually does not result in significant damage to the object of interest. Originally designed for metal quality control testing, Leeb testers are now also frequently used in geomorphological research (see, e.g., Alberti et al., 2013; Aoki & Matsukura, 2008) and, due to their easy operation in the field and the very short time of contact between the tester and the sample, qualify for hardness measurements on icy surfaces. The Leeb hardness test uses the rebound method. This method relies on deriving sample hardness from the loss of energy of a small impactor. A 3–5 mm diameter impactor with defined weight impinges on the surface of the test object at a defined speed of a few meters per second. The impact creates a plastic deformation of the surface, that is, an indentation, causing the impactor to lose part of its original kinetic energy. The velocities before and after the impact are measured using a contactless method. A spring-driven piston plunges toward the surface of the sample. The piston moves through a coil, causing an electric current with a voltage proportional to the velocity of the piston. The Leeb hardness (or Leeb number) HL is defined as

$$HL = 1,000\frac{|v_i|}{|v_r|} = 1,000C_r \tag{1}$$

(Leeb, 1979), where v_i and v_r are the impact and rebound velocities, respectively. C_r is the coefficient of restitution. The impact and rebound velocities are measured automatically.

We measured CO_2 ice hardness using a mobile Leeb hardness tester (Sauter GmbH, model Sauter HK-D). The main unit can be operated using seven different impact devices with various impactor sizes and energies, depending on the expected mechanical properties of the sample material. The so-called D-type sensor with an impact energy of 11 mJ is designed for general testing conditions. Henderson et al. (2019) chose this sensor for their hardness measurements of water ice. However, we found that the C-type sensor is a better choice for CO_2 ice measurements. Slabs of CO_2 ice usually have more cracks than H_2O ice samples and therefore break more easily. Because of these cracks, the sample areas suitable for hardness measurements are restricted. The C-type sensor has a lower impact energy of 2.7 mJ and a lighter tungsten carbide impactor (3 g vs. 5 g). Thus, significant damage to or breaking of the CO_2 ice sample becomes less likely. Furthermore, the lower impact energy of the C-type sensor allows shorter distances between two indentation centers and between an indentation center and the edge of tested sample compared to the D-type sensor, making it more suitable for smaller surface areas. In general, the C-type sensor is designed for small, light, and thin samples.

In our experiments we focus on the properties of CO_2 ice and the differences between CO_2 and H_2O ice. For comparison of our own data with Henderson et al. (2019) values for water ice, water ice hardness was measured with a Leeb tester using both the C-type and the D-type sensors.

2.1. Sample Preparation

We condensed CO_2 ice from the gas phase into a cylindrical tank whose base was cooled by liquid nitrogen and whose top was heated to a temperature above above 193 K to prevent clogging of the gas inlet, as described by Kaufmann and Hagermann (2017). As a consequence of the directional ice deposition caused by the thermal gradient inside the tank, we obtained clear slab ice showing no granularity (Figure 1). In some instances, patterns of cracks near the outer surfaces of the samples (which might be due to thermal expansion) could be interpreted as the delineations of individual crystals. These features were usually larger than 2 mm, a size similar to or greater than our impactor diameter. Six CO_2 ice slabs with a density of $1,513 \pm 75$ kg/m^3, diameter of 12 ± 0.8 cm, and an average height of 4.36 ± 1 cm were used as samples. Portyankina et al. (2019) found that the clear slab ice as used in our measurements is the most likely type

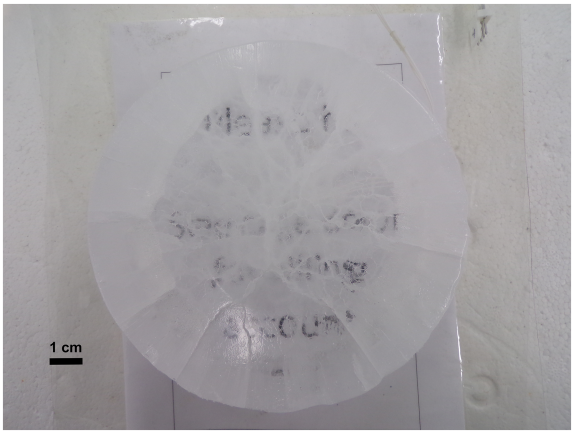

Figure 1. Example of a CO_2 ice block used as sample for the hardness measurements.

to form under Martian conditions. They also observed the formation of crystalline ice layers, albeit at much lower temperatures than commonly found on Mars.

Water ice samples were prepared by slowly freezing deionized water. We used Perspex tubes with different diameters as sample containers (d_1 = 12.4 cm and d_2 = 10.4 cm), obtaining cylindrical samples with heights between 2 and 4.2 cm. The water ice included a minor amount of air pockets and some samples also included cracks. However, all samples had a low porosity of only 1–2.5%. Only areas without visible cracks and inclusions were chosen for the hardness measurements. Before the measurements were done, the ice was polished to reduce the surface roughness. For recording temperatures during hardness measurements, a RTD sensor was frozen into both H_2O and CO_2 samples.

2.2. Measurements

The production process of CO_2 ice, combined with the material's high coefficient of thermal expansion, means that it is impossible to obtain crack-free ice slabs. Compact, transparent areas suitable for Leeb hardness measurements are usually smaller and rarer than in H_2O ice samples. As a result, the C-type sensor is more suitable for hardness measurements in CO_2; due to its lower impact energy, further cracking is avoided and the minimum surface areas required for accurate measurements can be smaller. We carried out hardness measurements on top of a crack in a sample in order to ascertain how cracks affect the hardness values measured. We found the values to be much lower than in the compact, clear regions of the sample. Sometimes, the effect would be such that hardness values could not be obtained at all because the instrument returned a measurement error.

Because our aim was to obtain hardness values for CO_2 as a function of temperature, we measured under the controlled conditions described below. However, as accurate temperature control is very resource intensive, we also made use of temperatures occurring naturally during the CO_2 slab production process or temperature regimes readily available in a freezer (which explains why our temperature error bars vary). Slab temperatures were measured using an RTD sensor placed approximately in the center of the sample. We were able to obtain hardness values over a temperature range from ~100 to 190 K.

Temperature control was achieved by placing the sample slab on an aluminum cold plate cooled to 186 K using LN_2 before the sample was placed on top. The sample was placed inside a Perspex tube, and the gap between sample and inner wall of the tube was filled with precooled glass beads, before the cold plate (and with it the sample) was slowly cooled further to 92.8 K (see Figure 2). A Styrofoam box covering the perspex tube was used to reduce frost formation by minimizing the flow of warm air onto the sample. Nevertheless, a thin layer of frost building up during the cooling process could not be avoided. The frost was wiped off before each measurement, leaving a minimal amount of frost on the surface. Since the diameter of the impactor and the depth of the crater obtained are much larger than the frost grain size and the height of the layer, the influence of frost on the hardness values is negligible. During cooling and subsequent measurements, the samples usually lost ~3% in volume and became less translucent, although samples tended to remain intact and could easily be removed and handled without breaking.

Figure 2. Setup for our CO_2 ice measurements. The cooling plate is connected via the pipes shown in the right lower corner to a LN_2 Dewar and a digital temperature control unit to stabilize the temperature. The image was taken after the measurements were done.

For hardness measurements of H_2O ice at temperatures of about 80 K a more simple, less time consuming approach for cooling the sample was chosen. For these measurements the sample was placed in a metal container with the gap between the sample and the inner wall of the container filled with glass beads. The container was then immersed directly into a bath of LN_2. Hardness measurements were carried out as soon as the sample temperature had stabilized. Since hardness values obtained using a Leeb hardness tester for H_2O ice have already been published (Henderson et al., 2019), measurements were only made in three temperature ranges: 243–247, 192–207, and 77–82 K, with the same causes for

Table 1
Hardness Values for CO_2 Ice at Different Temperatures

Temperature (K)	Leeb hardness (HL) mean ± st. dev.	No. of measurements
92.8 ± 1.8	359.1 ± 24.4	12
105.5 ± 0.3	384.6 ± 25.8	16
131.3 ± 2.9	315.4 ± 44.3	10
137.0 ± 1.2	288.3 ± 33.4	12
143.9 ± 3.1	304.5 ± 30.6	18
149.0 ± 2.1	277.1 ± 31.2	9
165.0 ± 1.5	220.2 ± 26.0	11
179.0 ± 0.8	200.1 ± 16.4	10
182.3 ± 2.2	197.2 ± 13.0	38
186.9 ± 4.0	196.2 ± 18.4	100

the variation in temperature uncertainties as described above. For comparison with Henderson et al., 2019's results, a few H_2O ice values were measured using both the C-type and D-type sensors.

The reason for the difference in experimental procedure was that the H_2O approach was not suitable for CO_2 ice because we found that nitrogen steam affected all samples considerably when it penetrated cracks in the ice slabs, resulting in softening or disintegration of the slabs. CO_2 slabs tended to have more cracks than H_2O slabs, although softening and disintegration could also be observed in H_2O samples with a high number of cracks.

For H_2O samples the hardness sensor was precooled when making measurement in the higher temperature ranges. In case of CO_2 ice samples, hardness values obtained with precooled sensor did not noticeably differ from measurements using a "warm" sensor; all values obtained were within the same error range. In order to ascertain that precooling the sensor does not affect the performance of the Leeb hardness tester, a simple series of experiments was carried out using a copper plate (20.5 × 20.5 × 1.5 cm) as a sample. The plate was kept at a constant temperature of 295 K. The sensor was cooled in three different ways: (i) the tip of the sensor was immersed in LN_2, (ii) only the sensor's impact body was cooled with LN_2, and (iii) the whole tester was stored in a freezer at 253 K for 35 min. The hardness values measured show no noticeable changes in comparison to the values measured with a sensor kept at room temperature. Average values are almost identical, with a standard deviation of 2.37 for the C-type sensor and 0.66 for the D-type sensor. As expected, the values obtained with the C-type sensor tend to be higher, in this case ~21%.

3. Results

The results of our measurements of Leeb hardness of CO_2 and H_2O ice are shown in Tables 1 and 2, respectively. Listed values were obtained using the C-type sensor unless otherwise noted and are graphically summarized in Figure 3. Comparing the values measured for CO_2 ice with both types of sensor at different temperatures, values measured with the C-type sensor are about 19% higher. In the case of H_2O ice this factor is slightly larger; values obtained with the C-type values are approximately 32% higher than the D-type values. Visual inspection of the ice surface after each experiment revealed small indentations of roughly the size of the impactor, to have formed, but no new fracturing occurred.

Table 2
Hardness Values for H_2O Ice at Different Temperatures

Temperature (K)	Leeb hardness (HL) mean ± st. dev.	No. of measurements
79.4 ± 1.1	440.0 ± 96.0	50
191.1 ± 2.3	246.0 ± 33.1	37
193.7 ± 3.1	230.2 ± 29.5	33
199.8 ± 6.5	234.9 ± 38.4	60
246.0 ± 2.4	212.1 ± 28.0	67

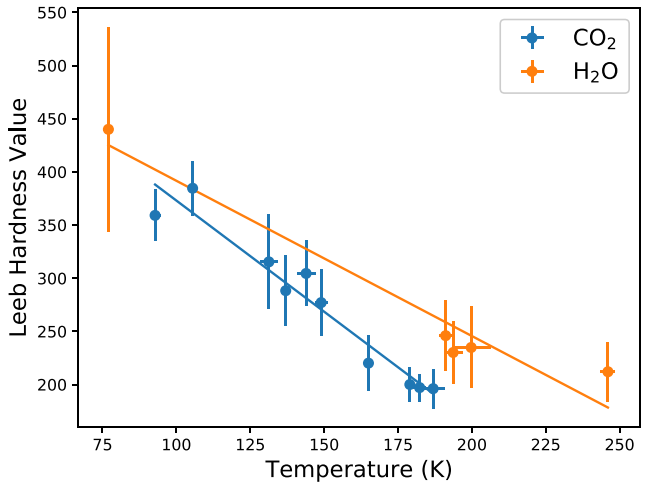

Figure 3. Leeb hardness test values for CO_2 and H_2O ice at different temperatures with the C-type sensor.

We found an approximately linear decrease in Leeb hardness with increasing temperature for both CO_2 and H_2O ice, as can be seen in Figure 3. An increase in hardness with decreasing temperature (away from the melting/sublimation point) is expected for icy materials and is fully in line with the H_2O ice hardness results of Henderson et al. (2019). The best fit relation for CO_2 is $HL = -2.089T + 582$, demonstrating a steeper temperature relation than water ice. CO_2 also has a larger thermal expansion coefficient than water ice (Mangan et al., 2017), potentially showing that its physical properties are more temperature dependent. When considering the uncertainties in Figure 3, however, the differences are not large.

4. Discussion

Hardness, as quantified by the Leeb values, represents the ability of a material to withstand indentation by plastic deformation. It can also be expressed in MPa and various other dimensionless scales (Vickers, Brinnel, etc.) related to each other by empirical conversion tables. A material's hardness is itself dependent on other, more intrinsic, properties such as its elastic stiffness (Young's modulus) and the stress at which it transitions from an elastic to plastic response (yield strength). The relation between these properties, and between yield strength and ultimate breaking strength, under compressive (such as in a hardness test), shear or tensile stresses, is complex and material dependent.

For the impact of a sphere onto a plate, where the solid plate only undergoes plastic deformation and no strain hardening or significant fracturing, the coefficient of restitution typically has a power law dependence on impact velocity and can be related to the dynamic yield strength Y by Johnson (1987) and Henderson et al. (2019)

$$Y = \left[\frac{\mathrm{HL}}{1000} \times \frac{E^{*\ 1/2}\ v^{1/4}\ \rho^{1/8}}{3.1}\right]^{8/5}. \quad (2)$$

Here, v is the impact speed (1.34 and 2 m s^{-1} for the C-type and D-type sensors, respectively), ρ is the target material density, and E^* is the reduced Young's modulus, given by

$$E^* = \left[\frac{1-\nu_I^2}{E_I} + \frac{1-\nu_T^2}{E_T}\right]^{-1}, \quad (3)$$

with $\nu_I = 0.18$ and $E_I = 621$ GPa Poisson's ratio and Young's modulus of the tungsten carbide impactor (Henderson et al., 2019). For the CO_2 ice target, $\nu_T = 0.544$ (Yamashita & Kato, 1997), and we obtain Young's modulus, E_T, from the temperature-dependent longitudinal wave velocity v_L, measured by Yamashita and Kato (1997), and density, calculated in equation (1) of Mangan et al. (2017), with the relation $E = \rho v_L^2$. The resulting Young's modulus over the relevant temperature range is shown in Figure 4, with a best fit curve of $E = -1.361\times10^5 T^2 + 2.985\times10^6 T + 1.47\times10^{10}$. For comparison, water ice at the same temperature (Gold, 1958) is ~1.1–1.3 times stiffer. This agrees with the results of Clark and Mullin (1976), who found CO_2 ice more likely to flow than water ice under the same stress.

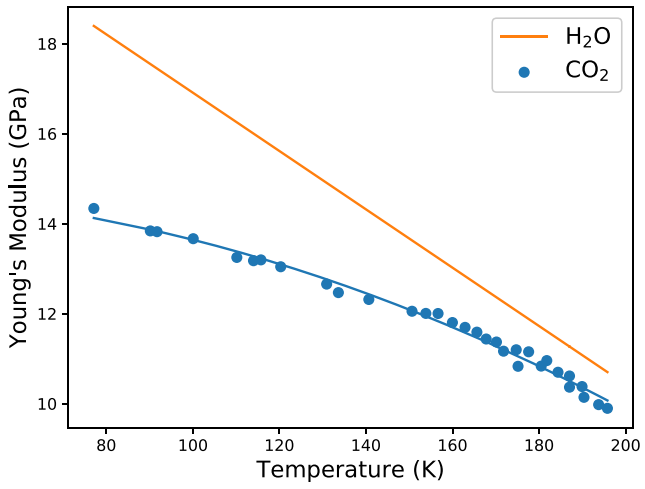

Figure 4. Young's modulus with temperature for water ice (Gold, 1958) and CO_2 ice (calculated from Yamashita & Kato, 1997, and Mangan et al., 2017).

With the above parameters we can calculate yield strengths of our ice samples. To do this, we must assume that they behave in a purely plastic way during the impact and that no strain hardening occurs, that is, the power law dependence of coefficient of restitution holds. For the former, the formation of small indentations in the sample of a similar size to the test impactor (3–5 mm) suggests plastic deformation, and no visible fractures are observed. For the latter there is no existing experimental evidence for CO_2 ice, while for water ice at higher temperatures,

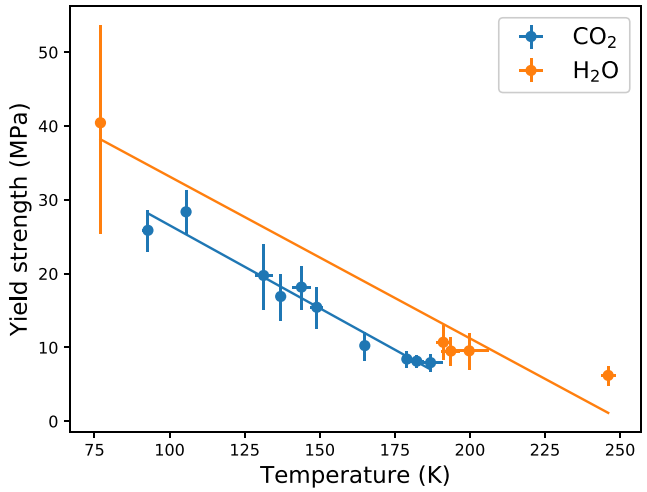

Figure 5. Calculated yield strengths for CO_2 and H_2O ice. The best fit line for CO_2 ice is $Y(\text{Pa}) = -2.247 \times 10^5 T + 4.902 \times 10^7$.

Higa et al. (1998) find that the coefficient of restitution does not follow a power law. In light of the lack of further data concerning CO_2 ice, and for ease of comparison with other works, we follow the method of Henderson et al. (2019) in assuming no strain hardening and in using the Johnson (1987) equation. We must advise caution when using the following results for absolute values. Nevertheless, relative values between the two ice types should always be applicable.

Figure 5 shows the results of equation (2). Our CO_2 ice samples have an estimated compressive yield strength of between ~10 and 30 MPa over the temperature range of ~100–200 K, with a similar temperature dependence to water ice but ~8 MPa smaller magnitude. Yield strength is typically smaller by a few times than ultimate strength σ (at which fractures will occur), so our results suggest a compressive fracturing strength for CO_2 ice of σ ~20–60 MPa. For comparison with an alternate method, the scaling relation $\sigma = 0.383H$ has been used previously for water ice (Epifanov, 2004), to relate ultimate strength, σ, to dynamic hardness, H, measured by the Brinell method. According to typical conversion tables for steel (e.g., ShapeCUT Steel, 2016), our Leeb hardness values correspond to Brinell hardness values $H < 130$, suggesting an ultimate compressive strength of $\sigma < 50$ MPa when using the above scaling relation. This is similar to the σ ~20–60 MPa estimate above, despite the uncertainty of using a conversion table for a different material. The relationship between tensile, shear, and compressive strength is also complex and material dependent, but in most materials it is found that compressive strength exceeds shear strength and that this in turn exceeds tensile strength. Rocks and geological materials, for example, typically have compressive strengths ~10 times larger than tensile (Sheorey, 1997), which suggests an ultimate CO_2 ice tensile strength of ~2–6 MPa from our results or < 5 MPa from the steel scaling relationship. This is in broad agreement with the suggested ~2 MPa tensile strength of water ice under Martian conditions used in previous works (Mellon, 1997).

As a further comparison, we show calculated yield strengths for our H_2O samples, taken with both the C-type and D-type sensors, alongside Henderson et al. (2019) values for slowly crystallized water ice in Figure 6. We find a very good match between sensor types, validating our use of the C-type sensor for the CO_2 ice, as well as broad agreement with Henderson et al. (2019) for H_2O ice, bearing in mind the large uncertainties in both experiments.

Thus, we can conclude by saying that at typical Martian temperatures, CO_2 ice is less hard than H_2O ice, as well as being less stiff (lower Young's modulus Gold, 1958 and larger creep coefficients Clark & Mullin, 1976; Durham et al., 1999) and with a similar or slightly lower yield strength (this work). It would therefore appear that CO_2 ice landforms should be more susceptible to fracturing than water ice features, when experiencing stresses such as from gas buildup in a solid-state greenhouse (Kieffer, 2007) or contraction from thermal cycling (Portyankina et al., 2012), the latter being especially relevant due to CO_2 ice's large thermal expansion coefficient relative to water ice (Mangan et al., 2017). This is, however, dependent on the rate of strain and physical scale of the relevant displacement. Our experimental results apply to a microscale, fast strain rate regime, as compared to slow processes such as glacial flow. At larger scales, grain boundaries and preexisting fractures will reduce the calculated yield strength, and at slow strain rates, the large CO_2 creep values will act to diffuse stress by plastic deformation rather than fracturing. Application of our results to real features should therefore be underpinned by a full viscoelastic model of the relevant problem. Our hardness measurement, relative to water ice, does represent an important input parameter for such models. We conclude with the following simple, order of magnitude, calculation regarding such modeling. Portyankina et al. (2010) simulate the buildup of gas by the solid-state greenhouse effect in Martian araneiform features and estimate fracturing after 1–20 days at 75°S using H_2O ice strengths of $Y = 50$ kPa

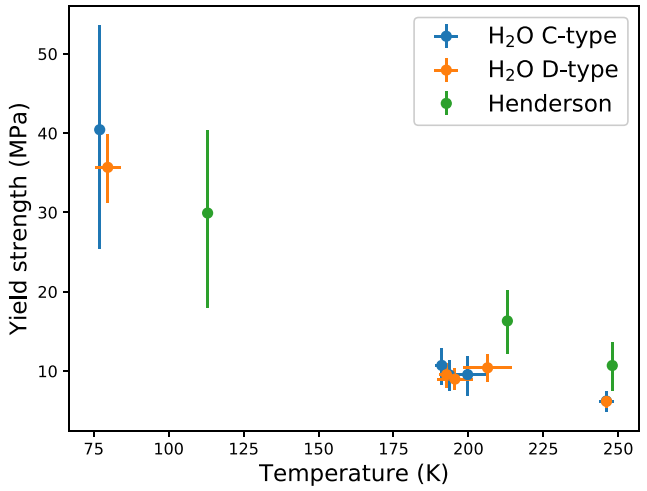

Figure 6. Calculated yield strengths for H_2O ice using two different sensor types and from Henderson et al. (2019).

to 100 MPa (note that there is a missing factor of 1,000, i.e., a missing "kilo," in their Figure 9 and associated description, G. Portyankina; personal communication, July 2019). At $T = 150$ K our results give $Y \approx 15.8$ MPa, which, when inserted into the relationship displayed in their Figure 9, would lead to fracturing on the 18th day of gas buildup.

5. Conclusion

We have measured the hardness of solid CO_2 ice directly in the laboratory with a Leeb hardness tester. We have also measured the hardness of water ice by the same method, confirming previous work for water ice. Our results indicate that CO_2 ice is slightly weaker, with Leeb hardness values ranging between ~200 and 400 (~10 and 30 MPa yield strength, assuming only plastic deformation and no strain hardening during the experiment), for typical Martian temperatures. This work supports the hypothesis that fracturing of solid CO_2 ice slabs (by basal sublimation or thermal stresses) plays an important role in morphological changes in the Martian polar regions. Future models of CO_2 ice fracturing should consider the timescales of plastic deformation when investigating surface-shaping processes.

Acknowledgments
The authors would like to acknowledge very detailed and constructive comments by W. Durham whose review helped substantially improve the original manuscript. Further helpful input from an anonymous referee was also much appreciated. This work was funded by STFC, Grant ST/S001271/1. N. A. is funded by the UK Space Agency, Grant ST/R001375/2. Data are available from DataSTORRE, the University of Stirling's data repository (Kaufmann et al., 2019).

References

Alberti, A. P., Gomes, A., Trenhaile, A., Oliveira, M., & Horacio, J. (2013). Correlating river terrace remnants using an Equotip hardness tester: An example from the Miño River, northwestern Iberian Peninsula. *Geomorphology*, *192*, 59–70. https://doi.org/10.1016/j.geomorph.2013.03.017

Aoki, H., & Matsukura, Y. (2008). Estimating the unconfined compressive strength of intact rocks from Equotip hardness. *Bulletin of Engineering Geology and the Environment*, *67*, 23–29. https://doi.org/10.1007/s10064-007-0116-z

Clark, B. R., & Mullin, R. P. (1976). Martian glaciation and the flow of solid CO_2. *Icarus*, *27*, 215–228. https://doi.org/10.1016/0019-1035(76)90005-1

Durham, W. B., Kirby, S. H., & Stern, L. A. (1999). Steady-state flow of solid CO_2: Preliminary results. *Geophysical Research Letters*, *26*(23), 3493–3496. https://doi.org/10.1029/1999GL008373

Epifanov, V. P. (2004). Rupture and dynamic hardness of ice. *Physics - Dokhlady*, *49*, 86–89. https://doi.org/10.1134/1.1686876

Gold, L. W. (1958). Some observations on the dependence of strain on stress for ice. *Canadian Journal of Physics*, *36*, 1265. https://doi.org/10.1139/p58-131

Henderson, B. L., Gudipati, M. S., & Bateman, F. B. (2019). Leeb hardness of salty Europa ice analogs exposed to high-energy electrons. *Icarus*, *322*, 114–120. https://doi.org/10.1016/j.icarus.2019.01.006

Higa, M., Arakawa, M., & Maeno, N. (1998). Size dependence of restitution coefficients of ice in relation to collision strength. *Icarus*, *133*(2), 310–320. https://doi.org/10.1006/icar.1998.5938

Johnson, K. L. (1987). *Contact mechanics*: Cambridge University Press.

Kaufmann, E., Attree, N., Bradwell, T., & Hagermann, A. (2019). CO_2 ice hardness and yield strength under Martian temperature conditions. University of Stirling. Faculty of Natural Sciences. Dataset http://hdl.handle.net/11667/138

Kaufmann, E., & Hagermann, A. (2017). Experimental investigation of insolation driven dust ejection from Mars CO_2 ice caps. *Icarus*, *282*, 118–126. https://doi.org/10.1016/j.icarus.2016.09.039

Kieffer, H. H. (2007). Cold jets in the Martian polar caps. *Journal of Geophysical Research*, *112*, E08005. https://doi.org/10.1029/2006JE002816

Kieffer, H. H., Titus, T. N., Mullins, K. F., & Christensen, P. R. (2000). Mars south polar spring and summer behavior observed by TES: Seasonal cap evolution controlled by frost grain size. *Journal of Geophysical Research*, *105*(E4), 9653–9700. https://doi.org/10.1029/1999JE001136

Leeb, D. (1979). Dynamic hardness testing of metallic materials. *NDT International*, *12*, 274–278. https://doi.org/10.1016/0308-9126(79)90087-7

Malin, M. C., Caplinger, M. A., & Davis, S. D. (2001). Observational evidence for an active surface reservoir of solid carbon dioxide on Mars. *Science*, *294*(5549), 2146–2148. https://doi.org/10.1126/science.1066416

Mangan, T. P., Salzmann, C. G., Plane, J. M. C., & Murray, B. J. (2017). CO_2 ice structure and density under Martian atmospheric conditions. *Icarus*, *294*, 201–208. https://doi.org/10.1016/j.icarus.2017.03.012

Mellon, M. T. (1997). Small-scale polygonal features on Mars: Seasonal thermal contraction cracks in permafrost. *Journal of Geophysical Research*, *102*, 25,617–25,628. https://doi.org/10.1029/97JE02582

Nye, J., Durham, W., Schenk, P., & Moore, J. (2000). The instability of a south polar cap on Mars composed of carbon dioxide. *Icarus*, *144*(2), 449–455. https://doi.org/10.1006/icar.1999.6306

Portyankina, G., Markiewicz, W. J., Thomas, N., Hansen, C. J., & Milazzo, M. (2010). HiRISE observations of gas sublimation-driven activity in Mars' southern polar regions: III. Models of processes involving translucent ice. *Icarus*, *205*, 311–320. https://doi.org/10.1016/j.icarus.2009.08.029

Portyankina, G., Merrison, J., Iversen, J. J., Yoldi, Z., Hansen, C. J., Aye, K. M., et al. (2019). Laboratory investigations of the physical state of CO_2 ice in a simulated Martian environment. *Icarus*, *322*, 210–220. https://doi.org/10.1016/j.icarus.2018.04.021

Portyankina, G., Pommerol, A., Aye, K.-M., Hansen, C. J., & Thomas, N. (2012). Polygonal cracks in the seasonal semi-translucent CO_2 ice layer in Martian polar areas. *Journal of Geophysical Research*, *117*, E02006. https://doi.org/10.1029/2011JE003917

ShapeCUT Steel (2016). Hardness conversion table. Retrieved 2019-06-19, from https://www.shapecut.com.au/wp-content/uploads/2016/01/ShapeCUT-Steel-Hardness-Conversion-Table.pdf

Sheorey, P. R. (1997). *Empirical rock failure criterion*. CRC Press.

Smith, R. L., & Sandland, G. E. (1925). Some notes on the use of a diamond pyramid for hardness testing. *Journal of the Iron and Steel Institute*, *111*, 285–294.

Yamashita, Y., & Kato, M. (1997). Viscoelastic properties of polycrystalline solid methane and carbon dioxide. *Geophysical Research Letters*, *24*, 1327–1330. https://doi.org/10.1029/97GL01205